INVESTIGATION OF FLIGHT DYNAMICS OF A CIVIL AIRCRAFT WITH ACTIVE HIGH LIFT SYSTEM

J.H. Diekmann, German Aerospace Center (DLR), Institute of Flight Systems

38108 Braunschweig, Germany

Abstract

In this paper ongoing research on the flight dynamic modeling and analysis of an aircraft with active high lift is presented. The considered aircraft is being designed with an aircraft multidisciplinary design and optimization tool (PrADO) and is a twin turboprop equipped with an active high lift system consisting of a Coandă surface flap whose knee is blown to enable boundary layer control. In this paper, a longitudinal model is derived from the first aerodynamic data available for this aircraft and used to make a first assessment of the flight dynamics of this aircraft configuration. In particular, the effects of the active high lift system on the trim conditions and the normal modes of the aircraft are shown, as well as a first assessment of the consequences of an active blowing system failure. A remarkable intermediate result is that with proper actions of the pilot (or the flight control system) such a failure seems to have significantly less severe consequences than initially feared.

NOMENCLATURE

C	Coefficient or derivative
C_μ	Jet momentum coefficient
$Error$	Relative error of model to CFD results
i	Incidence angle
k_1,k_2	Drag polynomial factors
l	Reference length (3.428 m)
$\dot{m}$	Mass flow
q	Pitch rate
q^*	Normalized pitch rate
q_∞	Dynamic pressure
S	Wing area (95 m²)
S_{HTP}	Horizontal tailplane area (24 m²)
V	Airspeed
x_{WHTP}	Lever arm of the HTP (16.23 m)
α	Angle of attack
ε	Downwash angle
ζ	Damping ratio
η	Elevator angle
Θ	Pitch attitude
v	Fluid velocity
τ	Transport delay of changes in wing lift at the horizontal tailplane

INDICES

0	Value for zero angle of attack
D	Drag
dyn	Dynamic value due to angular rates
jet	Jet of the blowing system
L	Lift
m	Pitching moment
PM	Pitching moment
TAS	True airspeed

ABBREVIATIONS

AHL	Active High Lift
Alt	Altitude
BLC	Boundary Layer Control
CC	Circulation Control
CFD	Computational Fluid Dynamics
CG	Center of Gravity
DFG	Deutsche Forschungsgemeinschaft (German Research Foundation)
DOC	Direct Operating Cost
DoF	Degrees of Freedom
FPA	Flight Path Angle
FS	Flap Setting
HTP	Horizontal Tailplane
MLW	Maximum Landing Weight
MTOW	Maximum Take-Off Weight
P2P	Peak to Peak
PrADO	Preliminary Aircraft Design and Optimization tool
RAC	Reference Aircraft Configuration
SFB	Sonderforschungsbereich (Collaborative Research Center)
STOL	Short Takeoff and Landing
TAS	True Airspeed
WFC	Wing Fuselage Configuration

1. INTRODUCTION

The continuously increasing number of flight movements leads frequently to saturation of airspace and airport capacity. Additionally today's air traffic forecasts predict the same increase of movements for the next decades. Therefore solutions to increase airport and airspace capacity must be found. A possibility is to better distribute the traffic over all airports, which would lead to a reduction of the workload increase (or even an absolute reduction) for central airport hubs and an increased use of smaller airports in the close vicinity of urban areas. These airports would be equipped with shorter runways and suitable for short and medium range flights. For such operations a new generation of quiet medium range aircraft providing short takeoff and landing capabilities is needed.

Active high lift (AHL) depending on blown flow control is a technology permitting to reduce the necessary runway

length due to the ability to fly at low airspeeds. It has been investigated over 50 years up to the present day [1]. In military aviation projects and prototypes have been initiated in order to achieve short takeoff and landing capabilities. Even though the theoretic results of blown flow control systems have been promising, it is remarkable that most concepts investigated and realized were different from flow control, e.g. vectored thrust or tilt rotor configurations. The only relevant military AHL aircraft is the Boeing C-17 transport aircraft [2]. In civil aviation this technology has not been considered for any aircraft to go into serial production or beyond prototype status in the last decades. Exceptions to this are the Antonov AN-72 and AN-74 using upper surface blowing. Since 2001 the latest redesigns of the AN-74 returned to a more conventional under wing engine configuration (AN 74TK-300) and AHL was abandoned. Civil applications of active high lift technologies are difficult to render economically viable when STOL is not required, due to development costs and certification reasons. Furthermore the integration of AHL systems also involves disadvantages, e.g. additional weight for the pressured air systems or for the redundant systems permitting to ensure safety.

Airfoils and flap systems of AHL systems are optimized primarily for STOL characteristics, but not for drag reduction in cruise flight. As for all complex system designs a tradeoff between various objectives and constraints must be made and a completely new design is necessary to take full advantage of an AHL system, which leads to a totally new specific configuration.

The DFG (German Research Foundation) initiated the SFB 880 project under the name “Fundamentals of High Lift for Future Civil Aircraft” in order to conduct fundamental and multidisciplinary research on high lift systems. The main focus lies on research on boundary layer control using a blown Coandă flap system as active high lift device. This device generates additional lift by blowing out pressurized air at the trailing edge of the wing over the knee of a specially shaped Coandă surface flap. The pressurized air can be provided by the engines using bleed air or by electrically operated microcompressors. The use of such technologies implies a special aircraft design as well as new materials and noise reduction techniques.

Using advanced design tools, the partners involved in the SFB 880 project can virtually create unconventional configurations and perform comprehensive AHL studies including complete redesign of the aircraft in order to maximize the benefits resulting from the integration of an AHL system. For instance, it can be assumed that an aircraft equipped with active high lift does not need as much additional flap area, fairings or wing chord for generating high lift performance that is comparable to more conventional aircraft configurations. Consequently the use of AHL permits to significantly downsize the wings and flaps and leads to adapt engine performance in order to have enough excess power for external systems.

On the other hand in order to reduce the necessary runway length for takeoff and landing an aircraft will have to be able to operate at low airspeeds. This leads to new requirements for the redesign and restricts downsizing ranges. The possible effects on the dynamic behavior and the handling qualities must be investigated thoroughly. Indeed, the controllability of the aircraft could be massively affected by the high lift system running at full power, due to the fact that the AHL system will not only influence lift, but also pitching moment, drag and wing-induced downwash at the horizontal tailplane (HTP) position.

The use of AHL also introduces a strong dependence of the lift generation on the engines. This dependence could lead to critical situations in case of engine failure, if not addressed properly during the design phase. The large flap deflections and the blown out air lead to strong downwash angles induced by the main wing at the HTP position. This change in downwash results in additional moments that affect the longitudinal behavior of the aircraft. Therefore, the consequences on the static and dynamic stability, the trimability and the flying qualities need to be analyzed.

In order to define the safety requirements for the different subsystems of an AHL-based aircraft, the consequences in terms of flight safety of AHL failures and malfunctions need to be determined. These safety requirements would then lead designers to adapt the system architecture, the level of redundancy, or to propagate them into additional requirements for some subsystems (for instance increase of actuator efficiency). When looking at the huge increases of the lift coefficient obtained through the use of AHL, it seems at first that AHL failures or malfunctions would often lead to catastrophic consequences. A first simplified analysis made in this paper shows that this is not necessarily the case, even though additional investigations based on data that are not available yet will be required to conclude definitively.

Apart from emergency and failure cases the flight performance of such an aircraft configuration will be different from standard civil aircraft with passive high lift devices and must be analyzed. In particular, the modified aircraft configuration including wing airfoil and flap redesign will not only affect takeoff and landing performance, but also the cruise performance. The special shape of a Coandă flap is not necessarily an ideal choice for a reduction of drag in cruise flight, thus cruise flight performance. On the other hand it is likely that savings in structural weight and the absence of fairings for complex flap systems can possibly cover these penalties of not cruise efficient shaping of the wing trailing edge.

These aspects considering flight dynamics, failure and emergency cases, as well as inflight performance will be part of the research program of the SFB 880 and will be investigated at a later stage of the project. Basis for all these investigations will be a nonlinear flight dynamic model incorporating the effects resulting from AHL devices. The first flight dynamic analyses that will be performed will focus on the impact of active high lift on the longitudinal motion of the aircraft, including trimability, stability and controllability tests.

2. MODELING

2.1. Reference Aircraft Configuration Design

The creation of a proper model for flight dynamics of aircraft with AHL systems has to be based on a comprehensive data set including for instance information about aerodynamics or geometry, which has to be

produced first. Therefore starting point for research on an especially designed AHL aircraft has to be a preliminary basic configuration designed from scratch. The benefits of an AHL system have to be considered for sizing of the geometries as well as engines and structural requirements. This has to be based on a first estimation for the additional lift, drag and moment increments in order to design a first configuration including the wing airfoil.

The overall configuration of the aircraft including sizing of aircraft body, wings, horizontal and vertical tailplane, as well as control surfaces has been performed with the preliminary design program PrADO [3]. The program has been developed by the Institute of Aircraft Design and Lightweight Structures of the Braunschweig Technical University (TU Braunschweig), which is a partner in the SFB 880 project. The PrADO program incorporates higher fidelity numerical methods for aerodynamics and structural analysis. The tool is not as much relying on empirical data as preliminary design processes often do. This capability makes it possible to estimate data for unconventional configurations or applications, like a new AHL system, where empirical data is missing or not applicable for the investigated technology or configuration. The process is divided into three steps, named Design Analysis, Parameter Variation and Optimization. Within these steps the resulting data is calculated iteratively until convergence of the parameters is reached.

In the framework of the SFB 880 project, PrADO will provide a highly comprising data set for the reference configuration which is defined by means of a set of constraints on payload, number of passengers, maximum takeoff and landing distances, engine type and number as well as type of high lift devices. The tool also takes the civil aviation safety requirements into account in case they are defined numerically. The design process with PrADO also includes an optimization of the expected direct operating cost (DOC). Figure 1 shows a cutaway drawing of the current Reference Aircraft Configuration (RAC). Though the exterior of the configuration does not look very different from common civil aircraft configurations, in detail the configuration is tuned for the use of the specified AHL device.

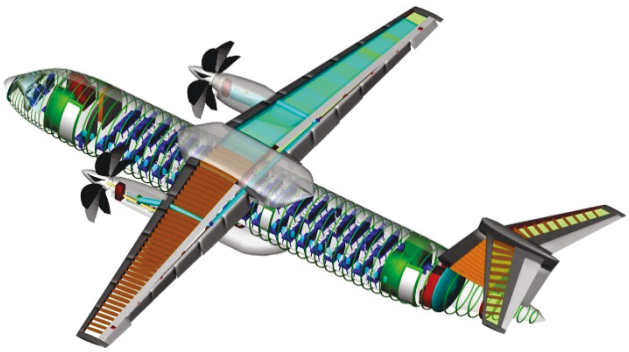

FIG. 1 Cutaway drawing of the Reference Aircraft Configuration [4]

The RAC data set contains additional information, like estimated weight data including weight limits (e.g. Maximum Take-Off Weight MTOW = 40.641 metric tons) and center of gravity (CG) position. For engine sizing detailed information like the propeller blade shape has been taken into account. As a result of the engine sizing an advanced thrust estimation sheet has been created including thrust limits as well as bleed air availability and fuel consumption for different flight phases, altitudes and flight speeds.

2.2. Flight Dynamic Model Structure

For numerical simulation a nonlinear six degrees of freedom (6 DoF) flight mechanical model is being developed. The AHL device is integrated into a comprehensive model structure, which is divided into different subsystems. The general model structure can be seen in the block diagram in Figure 2. The upper-left part of this diagram shows the main components that generate forces and moments (e.g. aerodynamics, gravity and integrated subsystems, for example engines or actuators). The total forces and moments are driving the 6 DoF differential equations of motion. The model architecture is based on the existing versatile modular architectures used at DLR, Institute of Flight Systems [5] and implemented using MATLAB/Simulink, which later is used to perform the numerical simulations.

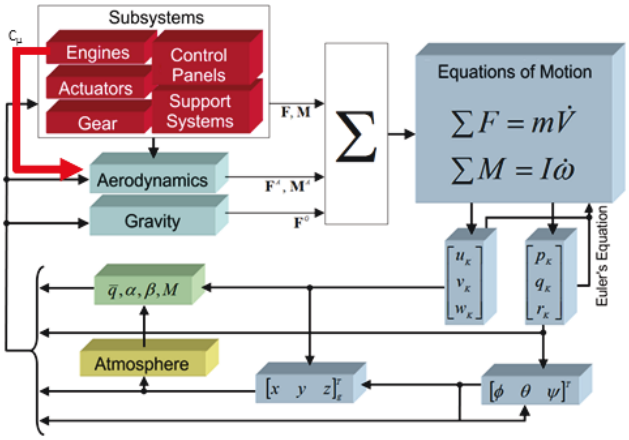

FIG. 2 Model structure

The engine subsystem is modeled for turboprop engines and contains nonlinear engine dynamics as well as thrust characteristic curves and the effect of slipstream over partial areas of the wing. Additionally the effects resulting from wind milling propeller feathering were integrated in the model using additional characteristic curves for these operating modes. The use of an AHL device introduces a coupling between the power generation in the engines and the high lift generation. Engine power is also not completely converted in thrust anymore. This led to a couple of slight modifications of the pre-existing model structure. The integration of the AHL system and the connection of engines and aerodynamic model are described in the next chapter.

2.3. Modeling the Active High Lift System

2.3.1. Description of blown flaps effect

A central element of the flight dynamics simulation is the aerodynamic model, which needs to include a model of the impact of the blown flap system on the aerodynamic behavior of the aircraft. Usually on civil aircraft, a mechanical high lift system involving flaps and slats is used to increase lift for start and landing. These mechanical high lift systems are increasing wing chord (and therefore also wing area) and/or camber. The complexity of these systems varies from single hinged flaps to multiply slotted extension flaps. For weight

reasons it is favorable to reduce the complexity as much as possible, which leads to systems with high deflection flaps rather than extension of multiple flap surfaces which often tend to become heavier due to necessary additional rails and fairings for support. Though it seems to be convenient to use simply constructed flaps with high ranges of deflection, these devices are not offering the same lift increases as more complex systems due to the detachment of the flow from the flap, which occurs at significantly smaller angles of deflection. As a result lift decreases almost immediately or the aircraft could even be stalled completely.

Active high lift devices like the internally blown Coandă flap are able to prevent this flow detachment even at high flap deflection angles. A possible shape can be seen in Figure 3, which also gives a flow field reaction on blowing over the knee of the flap.

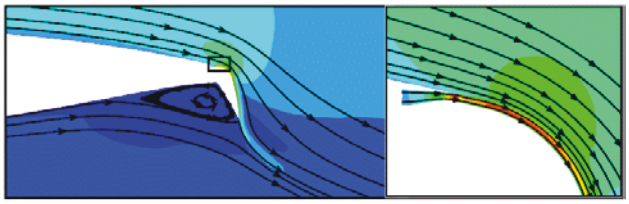

FIG. 3 Flow field example for a blown Coandă flap (source [6])

Apart from the shape of the flap, the ability to keep the flow attached to the flap depends mainly on the velocity and the mass flow characteristics of the jet that is blown over the knee of the flap. Besides flap setting a nondimensional parameter called the jet momentum coefficient C_{μ}, defined in Equation (1), plays an important role for the description of the flow conditions and thus of the resulting effects.

$$C_{\mu} = \frac{\dot{m}_{jet} \cdot v_{jet}}{q_{\infty} \cdot S} \quad (1)$$

The AHL has a major influence on all forces and moments involved in the longitudinal equations. Two ranges of jet momentum can be distinguished: for small $C_{\mu} < 4.5 \cdot 10^{-2}$ the boundary layer along the wing profile is affected which increases the lift, whereas for high $C_{\mu} > 4.5 \cdot 10^{-2}$ a new circulation is additionally induced. Hence the control of C_{μ} for small values can be described as boundary layer control (BLC) and for high values as circulation control (CC). Figure 4 shows qualitatively the influence of C_{μ} on lift coefficient. Due to the target of economic efficiency, the chosen high lift system shall use the upper range of BLC ($3.8 \cdot 10^{-2} < C_{\mu} < 4.5 \cdot 10^{-2}$). Recent results seems to indicate that the boundary between BLC and CC lies lower than initially expected, i.e. at $C_{\mu} \approx 3.3 \cdot 10^{-2}$ instead of the aforementioned value of $4.5 \cdot 10^{-2}$. Even though the results shown hereafter were produced with the initial range of values, the type of effects on the flight dynamic behavior will remain the same. Later on numerical values will be recomputed when the complete aerodynamic data set for the new range will be available.

In order to operate the AHL system energy has to be provided for generation of pressurized air. The desired range of jet momentum coefficient below values of the CC range is also more efficient due to a higher lift increment over required active blowing power ratio than for the CC case.

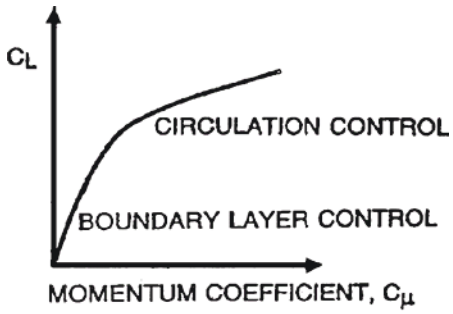

FIG. 4 Range of BLC and CC for a qualitative increase of lift over jet momentum (source [7])

2.3.2. Influence of C_{μ} control

Bleed air from the engines' compressor was chosen as the source for pressurized air. The usage of bleed air creates a direct coupling of lift to the power setting of the engine. This implies increased requirements for the engine performance to satisfy the usual operational limits for thrust while providing the required bleed air mass flow. Additionally, since taking too much bleed air from the engine can lead to a breakdown of the engine cycle, the maximum available air mass flow for active flap blowing depends on the current engine power setting. Below a defined minimum power setting the engines are not able to provide bleed air anymore and the AHL system has to be switched off. This also means that the engines cannot be operated in idle setting during approach with AHL system operative. Above this minimum power setting the mass flow that is provided for bleed air is kept constant.

The air mass flow is one of the central parameters for the additional lift generated by the AHL. It seems possible to use it as an additional flight control parameter. For instance, the available mass flow could be slightly varied using valves. Besides, the jet velocity can be influenced by controlling the blowing slot height. Therefore it might be possible to control the resulting jet momentum coefficient and to keep it in the defined BLC range. There are probably plenty of other possibilities to influence the resulting jet momentum and as thus the AHL-induced lift.

Within the SFB 880 project, electric microcompressors are being developed with the aim of decoupling engines from the pressurized air generation. This decoupling could provide greater flexibility for the architecture, in particular regarding safety level and safety assessment. Another possible advantage of these microcompressors would consist in having access to a wider range of air mass flow. Of course these microcompressors would necessarily rely on electric power generation provided by the engines or by the auxiliary power unit. These compressors could be spread along the trailing edge of the wing in order to locally produce pressurized air. This would also give the possibility of multiple redundancies as well as the chance to possibly influence the mass flow distribution along the wingspan.

2.4. Longitudinal Equations and Determination of the Numerical Values

For modeling of the aircraft aerodynamics a two point approach is used (see [8], [9], and [10]) following Equation (2).

$$C_L = C_{L,WFC}(\alpha) + \frac{S_{HTP}}{S} \cdot C_{L,HTP}(\alpha_{HTP}) \tag{2}$$

The aerodynamic coefficients of the wing fuselage configuration (WFC) are split from the aerodynamic coefficient of the horizontal tailplane (HTP) which is area scaled by $\frac{S_{HTP}}{S}$. Due to additional downwash effects at the position of the HTP the local angle of attack (α_{HTP}) is different from the main angle of attack (α). To compute a model for the wings downwash is required. This model will be introduced later, after the description of the WFC lift. The lift coefficients for the WFC can be split in the main lift of the WFC and the additional lift induced by the AHL system as described in Equation (3).

$$\begin{aligned} C_L = {} & C_{L0,WFC} + C_{L\alpha,WFC} \cdot \alpha \\ & + C_{L,WFC,AHL}(FS, C_{\mu 1}, \alpha) + \frac{S_{HTP}}{S} \cdot C_{L,HTP}(\alpha_{HTP}) \end{aligned} \tag{3}$$

The influence of the AHL system on the aerodynamics of the WFC with full flaps can be described approximately by a bilinear function of the momentum coefficient (C_μ) and the angle of attack (α), see Equations (4) and (5).

$$\Delta C_L(FS = 0°, C_\mu, \alpha) = 0 \tag{4}$$

$$\begin{aligned} \Delta C_L(FS = 65°, C_\mu, \alpha) = {} & \Delta C_{L,Flaps}(C_\mu = C_{\mu 1}, \alpha = 0°) \\ & + \frac{\partial C_{L,Flaps}}{\partial C_\mu}(C_\mu = C_{\mu 1}, \alpha = 0°)\ \Delta C_\mu \\ & + \frac{\partial C_{L,Flaps}}{\partial \alpha}(C_\mu = C_{\mu 1}, \alpha = 0°)\ \alpha \\ & + \frac{\partial C_{L,Flaps}}{\partial \alpha \partial C_\mu}(C_\mu = C_{\mu 1}, \alpha = 0°)\ \Delta C_\mu\ \alpha \\ & \text{with } \Delta C_\mu = (C_\mu - C_{\mu 1}) \end{aligned} \tag{5}$$

All the aerodynamic coefficients have been identified from 3D CFD calculations performed within the SFB 880 by other partners. Equation (5) consists of a first-order Taylor approximation of the dependence of the lift increase on both C_μ and α, in the neighborhood of the point $C_\mu = C_{\mu 1} = 4.5 \cdot 10^{-2}, \alpha = 0°$ for the full flap configuration. The numerical values for the constant term and the partial derivatives were obtained by a least-squares fitting of the CFD data. Due to the range of values that were taken into account for the CFD results used, this model represents well the effect of AHL for C_μ between $C_{\mu 1} = 4.5 \cdot 10^{-2}$and $C_{\mu 2} = 3.8 \cdot 10^{-2}$ and for attached flow. The aerodynamic coefficients for the full flap configuration but without active blowing were not computed yet and therefore are still missing in the model.

As already mentioned due to new aerodynamic results the range is likely to be adapted to lower C_μ values in the near future. Another effect of the AHL is a decrease of the maximum angle of attack: for full flap configuration with maximum blowing performance it decreases down to $\alpha_{max} = 4°$.This value defines the boundary of attached flow, which is not described in this model yet (no stall model). One of the next steps for the modeling process is to describe these nonlinearities taking also the variation of α_{max} with C_μ into account.

Apart from that, the aerodynamic forces and moments generated by the HTP are also modified while using the AHL system. Indeed, the AHL system strongly influences the downwash that is induced by the WFC and therefore the flow field encountered by the HTP is completely different. It is assumed that this downwash can be modeled as a function of the WFC lift. This assumption is based on the statement made in [11], that the downwash is depending on the circulation of the WFC. This assumption will be later verified using the CFD results.

Combined with the knowledge that lift is related to the circulation as well (see also in [11]) a relation between lift and downwash can be found. Equation (6) shows the affine (and delayed) function for the resulting downwash angle. This approach uses a simplification assuming that the relationship between lift and circulation is the same for every configuration and that this relationship is linear. It is further assumed that the downwash value at the HTP quarter-chord point can be used for the complete HTP (inhomogeneity of the induced flow field encountered by the HTP is neglected). Additionally the effect of the delay in the relationship between WFC lift and downwash angle is taken into account via the parameter τ which is defined by the distance between HTP and WFC divided by the airspeed.

$$\varepsilon = \varepsilon_{C_L=0} + \frac{\partial \varepsilon}{\partial C_L} \cdot C_{L,WFC}(t - \tau) \tag{6}$$

The corresponding coefficients have been extracted from the angles of the flow field at the desired point. These angles have been identified with the CFD results for the WFC. This way it is possible to describe the effect of the AHL system on the HTP by changes in downwash, which results in a change of the local angle of attack at the HTP α_{HTP}. The local angle of attack for the HTP α_{HTP} is described in Equation (7).

$$\alpha_{HTP} = \alpha - \varepsilon + i_{HTP} + \alpha_{dyn} \tag{7}$$

The incidence angle of the HTP i_{HTP} is set to zero for the modeling process. Anyhow being a part of the resulting local angle of attack (α_{HTP}) this angle is included in the calculations of the resulting local angle of attack for α_{HTP} as well. In this equation the dynamic angle of attack α_{dyn} is introduced. It represents the change of the local angle of attack due to the pitching motion and the distance between the HTP and the center of gravity. The resulting lift of the HTP $C_{L,HTP}$ including all dynamic and downwash effects can be calculated by Equation (8). The gradients for lift increase due to angle of attack $C_{L\alpha,HTP}$ and to elevator deflection $C_{L\eta,HTP}$ have been identified in the aerodynamic data of the CFD analysis.

$$C_{L,HTP} = C_{L0,HTP} + C_{L\alpha,HTP} \cdot \alpha_{HTP} + C_{L\eta,HTP} \cdot \eta \tag{8}$$

The results of the lift model for different angles of attack can be followed in Figure 5. The error with respect to the underlying CFD results is below $Error_{Lift}$ = 1.13 % for the range below the maximum angle of attack.

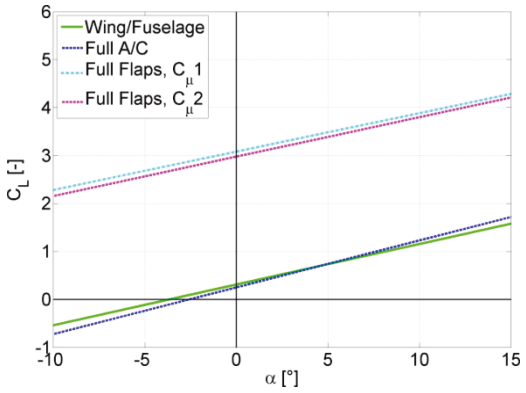

FIG. 5 Linear lift model

Besides the desired increase in lift, AHL has several additional influences on drag and pitching moment. The deflection and extension of flaps leads to a great increase of drag. For the used AHL system this increase can be observed as well. The induced drag has been modeled with a quadratic polynomial of the lift coefficient. The increment for flaps is assumed to be constant and the increment for jet momentum variations is modeled by a gradient for changes in jet momentum coefficient. Anyhow the resulting drag induced by the AHL system seems to be of high values, which can be explained to some extent by the induced drag depending on the high lift achieved. Another effect which is reflected in the drag increments for flaps and jet momentum is beside the additional parasite drag the effect of the suction peak at the trailing edge which is generated by the flap. Due to the high deflections this suction peak is turned into longitudinal direction and therefore generating additional forces in this direction.

The model for drag is described by Equation (9). The maximum error of drag with respect to the CFD is $Error_{Drag}$ = 3.02 % (again for the range below maximum angle of attack).

$$C_D = C_{D0_{WFC+HTP}} + k_1 \cdot C_L + k_2 \cdot C_L^2 + \Delta C_{D0_{Flaps}} \cdot FS + \Delta C_{D0_{\Delta C_\mu}} \cdot \Delta C_\mu \tag{9}$$

The results of the drag model for different angles of attack and configurations of the RAC can be seen in Figure 6.

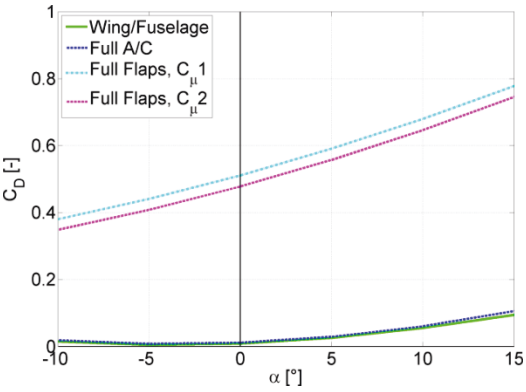

FIG. 6 Drag model

Standard mechanical high lift systems often generate a large nose down pitching moment. It might be explained by the development of a suction peak at the trailing edge of the wing respectively at the knee or bending point of the flap. This effect could possibly be increased by AHL devices. The expectation of generating even more nose down pitching moment would seem to be reasonable, by increasing flap deflection combined with blowing systems and therefore producing an increase in suction strength.

The expected effect has been confirmed by CFD results in terms of a large negative value for the pitching moment increment induced by the flaps. However, the pitching moment which can be seen in Figure (7) has a lower gradient than the clean configuration of the aircraft. This can be explained by the strong downwash the HTP is exposed to. Indeed the high values for lift in the full flaps configuration with AHL system operative induce a remarkably strong downwash. This leads to an unusually large nose up pitching moment, which is even exceeding the great nose down pitching moment of the AHL system in magnitude. The figure also shows the impact of a variation of jet momentum coefficients leading to a slight increase of the pitching moment gradient ($C_{m\alpha}$) for decreasing jet momentum coefficients.

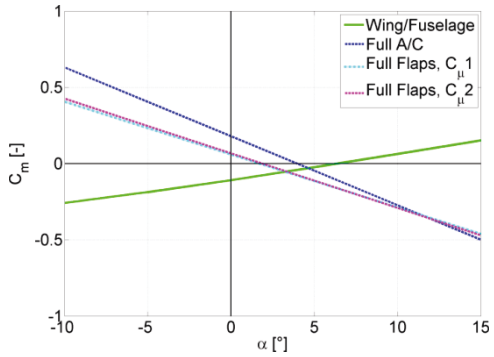

FIG. 7 Pitching moment model

The model for pitching moment is provided in Equation (10).

$$C_m = C_{m0_{WFC}} + C_{m\alpha_{WFC}} \cdot \alpha - \frac{S_{HTP}}{S} \cdot \frac{x_{WHTP}}{l} \cdot C_{L_{HTP}}(\alpha_{HTP}) \Delta C_m(FS, \alpha, C_\mu) + C_{mq_{WFC}} \cdot q^* \tag{10}$$

with

$$\Delta C_m(FS = 0°, \alpha, C_\mu) = 0$$

$$\Delta C_m(FS = 65°, \alpha, C_\mu) = \frac{\partial C_m}{\partial FS}(\alpha = 0°, C_\mu = C_{\mu 1}) \cdot FS + \frac{\partial C_m}{\partial \alpha \partial FS}(\alpha = 0°, C_\mu = C_{\mu 1}) \cdot FS \cdot \alpha + \frac{\partial C_m}{\partial C_\mu}(\alpha = 0°, C_\mu = C_{\mu 1}) \cdot \Delta C_\mu + \frac{\partial C_m}{\partial \alpha \partial C_\mu}(\alpha = 0°, C_\mu = C_{\mu 1}) \cdot \Delta C_\mu \cdot \alpha$$

The aforementioned effect of the downwash is not directly observable in this equation: it is part of the α_{HTP} term. The calculation of the moment coefficient induced by lift of the HTP is realized by multiplication with the normalized lever arm $\frac{x_{WHTP}}{l}$ which is the horizontal distance between the geometric neutral point of the HTP and the moment reference point over the reference length. The moment reference point for all coefficients has been chosen to be above the centerline of the aircraft at the vertical and longitudinal position of the main wing's quarter chord. In

order to integrate the dynamic reaction of the WFC to pitching rates, another coefficient for the normalized pitching rate $q^* = \frac{l}{V} \cdot q$ has been used which was also identified by CFD results for WFC.

The maximum error with respect to the CFD results rises up to $Error_{PM}$ = 20.79 % which seems to be large, at first. In reality, this relative error is not critical because these errors occur for very small values: the maximum absolute error is only $Error_{PM\ Absolute}$ = 0.0018.

All described effects of an AHL system on aerodynamics and engines are implemented into the simulation model. The resulting model modifications are assuming that effects of the AHL system on lift and pitching moment show an approximately affine behavior for the attached flow domain. Although being a quite simple approach, the impact on aircraft trimability, stability and controllability, as well as coupling effects of lift and thrust will become obvious. Of course extensions of this model to include a proper description of the nonlinear effects close to maximum angles of attack and after will be required for all configurations and air mass flows. Another important aspect will be the identification of slipstream effects on lift, drag and pitching moment. More complete CFD results will be available soon and be used for improvement of the current model.

3. FIRST FLIGHT DYNAMIC ANALYSES

Although the validity domain of the current model is restricted, the first flight dynamic analyses for the reference aircraft configuration can be performed, taking care of using the model only inside this domain. Note that during regular flight the aircraft will stay in this domain.

3.1.1. Trimability

First step for flight dynamic simulations is the analysis of the trimability of the flight dynamic model. As a first result of the trimming investigation for the longitudinal motion, it can be determined, if the aircraft is trimable at different attitudes, velocities or flight path angles (FPA). Important results can be the settings for thrust or incidence angle of the HTP (i_{HTP}). Especially for flying at low speeds the setting of the trimmed HTP incidence angle can give information about the sizing and resulting efficiency of the HTP. This needs to be sufficient for keeping the attitude constant at low flying speeds as necessary for short take-off and landing procedures.

For the following simulations two trim points were generated for symmetric unaccelerated horizontal flight. The lower speed boundary is given by the stall speed for angles of attack at α_{max}=4° in full flaps with blowing active configuration. The HTP incidence angle margin is defined for the RAC by $|i_{HTP}| \leq 8°$. The center of gravity can be moved along the centerline of the aircraft. For the given simulations it is set below the geometric neutral point of the wing in longitudinal direction. The trim point parameters of the first example show the values for the cruise condition. Amongst others angle of attack (α), incidence angle of the HTP (i_{HTP}) and engine power lever position controlling engine performance ($Throttle$) are the important trim variables, which can be adjusted by the trimming routine. For cruise airspeed of VTAS = 220 m/s and cruise altitude of 10600 m (34776.0 ft) the aircraft is trimmed at the values given in the Appendix (Table 2: Case 1). The resulting values indicate a good trimability of the aircraft for this flying condition. The angle of attack (α) is quite moderate and the trim angle of the HTP (i_{HTP}) is moderate which provides margins in both directions.

Another example gives the values of a trim point for slow flight condition at low altitudes. The aircraft operates in full flaps with blowing active configuration. In order to prevent a violation of the α_{max}=4° criterion in dynamic simulation including phugoid motion, the trim point has been chosen below maximum. Nevertheless the chosen point is close to the operational limits of the aircraft. The resulting values for the trim parameters can be seen in Case 5 of the Appendix Table 2. The trimming results fulfill the given criteria and show even normal small deflection values for HTP trim angle which is remarkable for very slow airspeeds. Various trim points can be found in Table 2 of the Appendix. Besides the trim points for the simulations (Case 1, Case 5) of section 3.3., additional trim points for maximum take-off weight and maximum landing weight at different angles of attack (α) are given in order to get an impression of the trimability of the aircraft. For all given trim points the trim angle of the HTP (i_{HTP}) is far away from maximum values. Note the large negative values for (α_{HTP}) for the full flaps with AHS cases (cases 4 and 5), that result from the strong lift of the WFC and permit to compensate the pitching down moment of the WFC in that configuration.

3.2. Stability

The stability of an aircraft can be divided into static and dynamic stability. In the attached flow domain ($\alpha << \alpha_{max}$) the static stability of the aircraft can be proven by checking a sign condition on the resulting gradient of the pitching moment with respect to the angle of attack ($C_{m\alpha}$<0). In Figure 7 the aircraft pitching moment coefficient is plotted against the angle of attack for various configurations (each time with i_{HTP} = 0). The gradient of the clean or cruise configuration of the aircraft is indeed negative ($C_{m\alpha}$<0), and thus the aircraft is statically stable. It should be noted that overall (i.e. flaps and jet momentum together) the AHL system reduces the static margin of the aircraft. Since $C_{m\alpha}(C_{\mu 1}) > C_{m\alpha}(C_{\mu 2})$ with $C_{\mu 1} > C_{\mu 2}$ a reduction of jet momentum seems to have an effect in reverse direction. Anyhow the observed difference is very small and no real issue should result from this effect even if much larger C_μ would be considered. It is quite remarkable, that even though the identified pitching moment coefficient increment values due to the AHL system for the WFC are rather large $\frac{\partial C_m}{\partial FS}\left(\alpha = 0°, C_\mu = C_{\mu 1}\right) \cdot FS = -1.33$ and $\frac{\partial C_m}{\partial C_\mu}\left(\alpha = 0°, C_\mu = C_{\mu 1}\right) \cdot \left(0.038 - C_{\mu 1}\right) = 0.033$, the global effect is in the opposite direction. This is due to a very large change of HTP lift force, which is a consequence of the strong change of the downwash (itself resulting from the massive lift increase). In total, this leads to the described reduction of the static stability of the aircraft in full flaps configuration with active blowing system. The fact that these effects compensate each other partly permits to avoid trouble for the trim of the aircraft and the trim deflections of the HTP shown in the appendix are small and very similar for clean and full flap with AHL configurations.

For dynamic stability a quick indicator can be the aircraft reaction on an elevator deflection pulse. Dynamically stable aircraft react on this input with the phugoid motion. The phugoid has a low frequency and its amplitude slowly declines over time. The second characteristic mode is the short period motion, which is a highly damped oscillation in angle of attack at a higher frequency. The greater the damping and frequency of phugoid and short period motion the higher is the dynamic stability of the aircraft in the longitudinal motion. The damping of the well damped short period motion mainly depends on the lift generation of the HTP due to the dynamic angle of attack (α_{dyn}) which results from pitch rates around the center of gravity. This dynamic angle is not influenced by the AHL system, hence the damping term of the short period motion will stay almost constant. Note that due to the fact that the AHL system reduces (in magnitude) $C_{m\alpha}$, this would correspond to a slightly increased short period damping ratio. Therefore the following simulations will focus on the influences of the AHL system on the phugoid motion. In order to quantify the results for dynamic stability, analytical investigations will be performed in the near future, including locations of the corresponding poles and zeros in the complex plane.

3.3. Dynamic Simulations for Phugoid Analysis

The first simulation test is a one-second elevator pulse of η = 1° at Time = 20 s. This way both dynamic modes of the aircraft can be induced in order to check for dynamic stability. Figure 8 shows the response to this input of the angle of attack (α), pitch rate (q), pitch attitude (θ), true airspeed (V_{TAS}) and altitude (Alt). In the first 20 seconds, it can be observed, that the aircraft was trimmed correctly. After the elevator pulse the typical elevator induced peaks in angle of attack (α), pitch rate (q) and pitch attitude (θ) can be noticed, which are transitioning into the sinusoidal behavior of the phugoid motion. The expected following low frequency sinusoidal behavior can be well observed for pitch attitude (θ), true airspeed (V_{TAS}) and altitude (Alt). For all given parameters a decline of the oscillation amplitude can be noticed. The short period motion is scarcely observable in this figure due to its much faster and damped response compared to the phugoid and to the very long time period represented (500 seconds).

For the slow airspeed trim point (Case 5 in Table 2) the simulation procedure has been executed similarly to the cruise trim point 1 in Table 2. Again and as expected, the values do not vary during the first 20 seconds. Figure 9 shows the results of the second simulation.

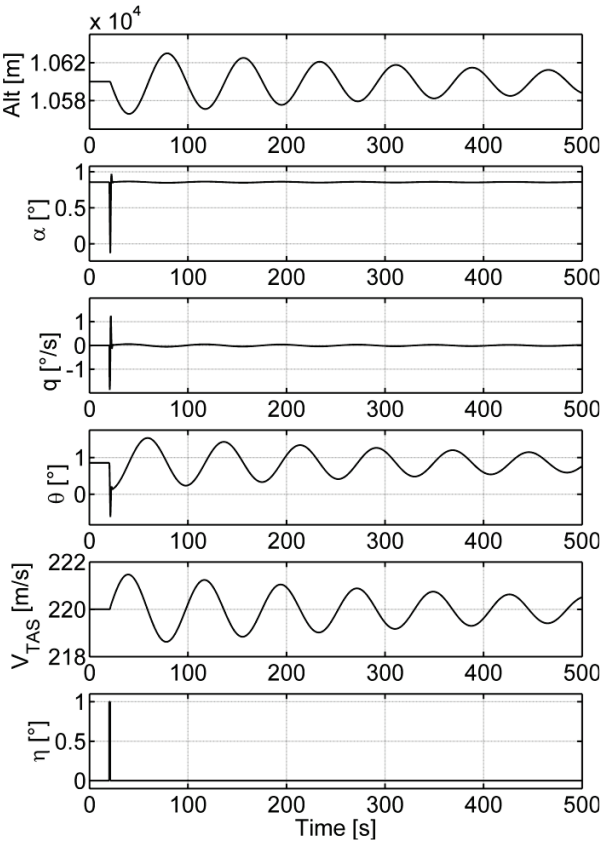

FIG. 8 Simulation results for elevator pulse in cruise configuration

The one second elevator pulse of η = 1° at Time = 20 s leads to the typical peaks in angle of attack (α), pitch rate (q) and pitch attitude (θ) as also noticed in the first simulation. Unlike for the first trim point the deviations from trimmed values for the second trim point are considerably less. The results for the second trim point also indicate lower amplitude for the following sinusoidal behavior of the given parameters. The decline of the oscillation amplitude appears considerably quicker, so that the values almost completely returned to the initial trim values at Time = 200 s. This behavior is rather uncommon. The phugoid motion is significantly faster than in the first case, which is a logical consequence of the lower speed. However the damping ratio is unusually large and the reasons for that will be explained hereafter.

The jet momentum coefficient can influence the damping of the phugoid. Indeed, due to its dependency on airspeed the jet momentum coefficient C_μ varies during the phugoid oscillation, modifying the aerodynamics at the same time. This creates an additional coupling between lift and airspeed, which is able to influence the dynamic stability of the phugoid motion. The question of the role played by this coefficient is also related to the question whether the air mass flow should be kept constant (for example by means of a controller) or left variable. On the other side by controlling it actively an additional degree of freedom for the control would be obtained, just as with Direct Lift Control (DLC) systems.

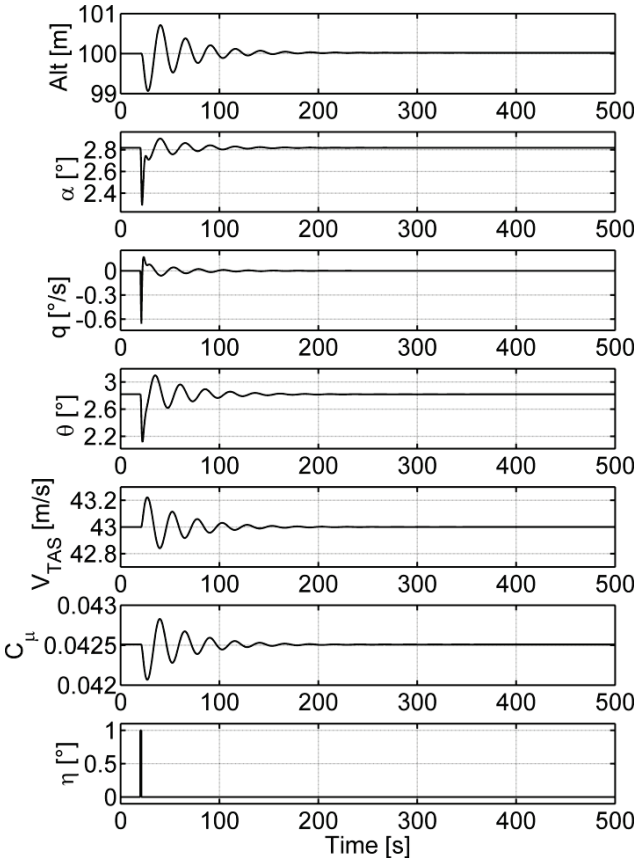

FIG. 9 Simulation results for elevator pulse in full flaps with blowing active configuration

For the analysis of the described effects the phugoid motion is excited this time by initializing the simulation with an airspeed different to the trimmed value of the chosen flight case. Compared to the previous simulations, this procedure reduces the excitation of the short-period motion. The chosen altitude is 1500 m and the initial airspeed is defined as 90 % of the trimmed value. The results of the two simulations (one per combination of parameters) are presented in Figure 10.

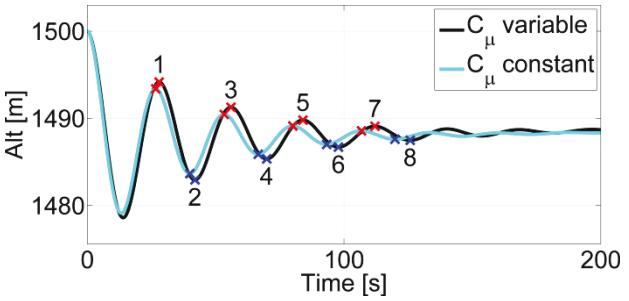

FIG. 10 Phugoid for constant/variable thrust and jet momentum coefficient

A constant jet momentum seems to increase the damping of the phugoid, which is indicated by the quicker decrease of the oscillation amplitude for constant values compared to variable ones. In order to establish a first quantification for these results a peak to peak ratio has been calculated for the four oscillations. The maximum peaks (red crosses) and the minimum peaks (blue crosses) have been numbered in sequence. The calculation has been carried out for peaks $n = [1; 3; 5]$. The calculation can be comprehended by Equation (11). To get the equivalent damping ratio Equation (12) is used.

$$P2P_{Ratio} = \frac{Alt(n+2) - Alt(n+3)}{Alt(n) - Alt(n+1)} \tag{11}$$

$$\zeta = \frac{1}{\sqrt{1 + \left(\frac{2\pi}{\ln(P2P_{Ratio})}\right)^2}} \tag{12}$$

As expected for this locally almost linear system the peak to peak ratio stays constant for the different calculated points. The mean value has been taken in order to describe the overall peak to peak ratio and to calculate the equivalent damping ratio. The resulting mean values for the peak to peak ratio can be seen in Table 1.

Case	Peak to Peak Ratio			
	Min	Mean	Max	ζ_{Mean}
C_μ *variable*	0.516	0.523	0.528	0.103
C_μ *constant*	0.454	0.463	0.469	0.122

TAB. 1 Peak-to-Peak ratio of the phugoid

These ratios give a good indication about the damping effects of variable thrust and jet momentum coefficients. It can be recognized that holding the jet momentum constant increases the damping of the oscillation. Anyhow the given results do not explain the unusually high damping ratio observed for the phugoid in full flap configuration. Indeed, by deriving an analytical expression for the natural modes of an airplane a relation between the damping ratio and the inverse lift to drag or glide ratio can be found [9]. Being in a normal range for civil aircraft in clean configuration of L/D > 14, the damping was also not surprising. However, the lift to drag ratio for the full flaps configuration system is unusually low L/D < 6, which explains very well the unusually large damping ratio that this aircraft in full flap with AHL exhibits. A similar tendency (though with much lower amplitude) is observed with a classical high lift system, in particular when it strongly increase the drag.

3.4. Analysis of Aircraft Reaction to AHL Failure

As mentioned in the beginning it seems presumable that failures of the AHL system case could lead to catastrophic consequences and therefore to stringent requirements for the safety level of many components of the system. Due to the numerous couplings between the aircraft motion and the AHL as well as between the AHL and the aerodynamics of both the WFC and the HTP, the exact consequences of such a failure are not so easy to predict. In order to get a first idea of these consequences, another simulation with an AHL failure has been carried out. Of course the loss of the AHL will lead to a significant loss of lift and altitude. This simulation aims to quantify this loss of altitude, assuming that the pilot is taking actions to counter it shortly after the failure occurred. The simulation will be initialized in a trimmed state at 1000 m altitude at low airspeed (V_{TAS} = 50m/s) and for unaccelerated horizontal flight. At time t=1s the AHL system fails (jet momentum coefficient is set to zero), due to a complete loss of pressurized air mass flow. The resulting aircraft behavior can be seen in Figure 11. The following process is assumed to be ideal, which means throttle is instantly set to Throttle = 100 % and Flaps are retracted from

Flaps = 65° to Flaps = 0° without any dynamic model for flap actuators or transition. The immediately reached new position for the flap is disputable, but was taken in this scenario because no data is available yet for intermediate flap positions or for full flap with no active blowing: at this stage of the model development, any other scenario would have been even less physically correct. The dynamic models for elevator, engine and incidence angle of the HTP still remain active. For the purpose of this analysis, a very basic controller has been integrated in order to control the elevator input and to achieve the target reference angle of attack of α = 10°. The controller is activated 0.77 seconds after the fault. The chosen reference value for alpha is assumed to be still below the maximum angle of attack for the clean configuration. Since the angle of attack at which C_{Lmax} is reached for the clean configuration is not known yet, this value was chosen instead. At Time = 10 s the pitch angle of the HTP is changed as most autotrim functions would do. The required change of trim is Δi_{HTP} = -5°.

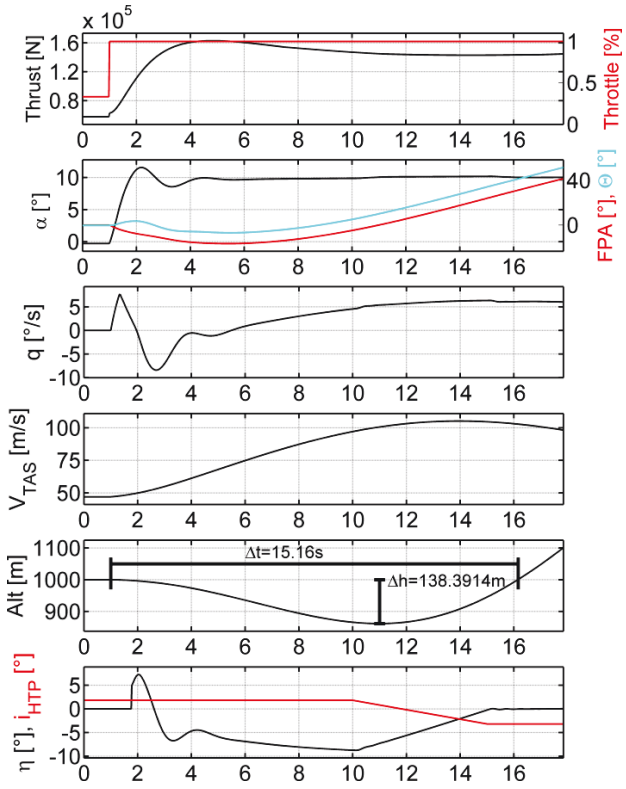

FIG. 11 Aircraft behavior for an AHL system failure

For the given scenario the angle of attack does not exceed α = 11.56°, which still can be considered as relatively uncritical. The original altitude of 1000 m is regained after Δt = 15.16 s. During this period of time the maximum loss in altitude has been Δh = 138.39 m. For the resulting thrust a small step after t = 1 s can be recognized, which is related to the increased efficiency of the engines without bleed air extraction. The deactivation of the AHL induces very quickly a positive nose up pitch motion, which can be explained by the sudden loss of the nose down pitching moment of the AHL system, which has been counteracted by the HTP whose nose up pitching effect is still active due to the delayed reaction on the downwash. Even though this first reaction of the aircraft is quite strong (and could surprise pilots), the situation seems to be controllable, which is indicated by the resulting elevator control inputs, which are far away from the deflection limits of $\eta_{max} = \pm 15°$. Note that the controller is activated 0.77 seconds after the fault and counteracts immediately the positive pitch rate: the controller did not provoke or contribute to this pitch up motion. The thrust seems to exhibit an overshoot. The very first part of the thrust response is indeed due to the engine dynamics, but then the variations of net thrust are caused by the rather strong variations of speed and altitude. Due to the control actions performed (maximum thrust, high angle of attack) a large climb rate is obtained rapidly. The flight path angle is almost 40° at the end of the simulation.

4. DISCUSSION

It has been possible to prove the aircraft's static stability for the investigated flight cases. Even though this aspect was not surprising the amplitudes of the moments acting on the various parts of the airframe seem unusually large. Two effects namely the induced pitching moment of the AHL system and the strong downwash result in a counteracting pitching moment induced by the HTP, which leads to a reduction of the gradient hence static stability compared to the cruise configuration. It seems like this effect could put a certain risk on aircrafts behavior once this coincidence vanishes unilaterally. For instance a system failure of the AHL system would not only lead to an immediate loss of lift but also to a loss of pitching moment. This change in downwash would change the lift of the HTP with a transport delay. This leads to a short period of time where only one of the two moments that were counteracting each other is still present while the other counterpart vanished already. This predicted behavior is also reflected by the system failure simulation which shows a quickly increasing nose up pitching rate directly after the AHL system failure. Anyhow this initial pitch up movement seems to be controllable and it will be interesting to have a closer look at the transition process of the aircraft and to the possible pilot reactions induced by this motion. In the presence of modern control laws, this reaction of the aircraft could probably be alleviated. Another aspect considering the aforementioned two large counteracting moments is to check the structural load induced (and the consequences for the structural weight). The large values for α_{HTP} could also lead to flow separation at the HTP during maneuvers. The dynamic stability of this aircraft does not seem to be an issue. An interesting outcome of the analysis is the significant increase of the phugoid damping ratio for the full flaps configuration. This finding leads to several new interesting questions considering handling qualities during manual approach situations. A rather fast and well damped phugoid could be appreciated by some pilots and disorientate others. In particular, a higher oscillation frequency should be easier to perceive for human senses but could require quicker actions. The system failure simulation has been conducted in order to get a first impression of how hazardous such situations might be. Contrary to the first expectations, i.e. that a loss of the system could lead to extreme upsets, stall or other uncontrollable situations, the aircraft seems to remain relatively well controllable (under the simplifying assumptions that the current state of the model forced to make). The loss of altitude does not seem to be as catastrophic as initially feared. Nevertheless in case of a

failure at very low altitude this failure would still remain catastrophic.

The definition of safety requirements including safety margins for probabilities of occurrence of such cases will have to be made in the following part of the project. Note that the high lift system might also have intermediate flap positions enabling to generate significantly more lift than the clean configuration without requiring the active blowing. The altitude loss could therefore be significantly lower than in the simulation presented in this paper. The transition from full flaps to clean configuration as well as from clean to full flaps during descent and approach must be better simulated and the corresponding flight procedure investigated. As mentioned initially the given trim points and dynamic simulations are based on preliminary aerodynamic data and idealized assumptions for the aerodynamic model. Anyway the results are able to illuminate several significant influences of the AHL system on the flight dynamic behavior of this aircraft. Effects like propeller slipstream have not been considered yet, but will be integrated soon once the respective CFD results for identification are available.

5. CONCLUSIONS AND OUTLOOK

The present paper gives a first impression of flight dynamics of an aircraft with active high lift system. The analysis of the pitching moment indicated an increase of $C_{m\alpha}$ due to the active high lift system but the aircraft is still largely statically stable. A closer look disclosed a counteraction of two strong moments initiated by the system. The nose down pitching moment of the active high lift system has been neutralized by the even more dominant downwash resulting in a nose up pitching moment of the horizontal tailplane. Apart from the consequences for the structure, this plays a major role in the pitch reaction of the aircraft after an AHL failure. Most significantly the damping of the phugoid for full flaps configuration needs to be mentioned. Due to the particular low lift to drag ratio for this configuration the phugoid declined remarkably quicker than expected. Additional simulations determined the impact of the active high lift system on the dynamic stability in terms of frequency and damping ratio of the phugoid motion. It could be pointed out that the natural variations of jet momentum of the active high lift system have a slightly destabilizing influence.

Simulation results for an active high lift failure case do not lead to a behavior as dramatic as initially feared. It seems that altitude loss could be contained in a quite acceptable range. Nevertheless failure scenarios must be investigated further as soon as enough data will be available. In the near future further investigations considering control efficiency and aircraft performance will be conducted. Additional effects like propeller slipstream and nonlinear aerodynamics will be introduced soon. This will lead to a better understanding of the impact of active high lift systems on the aircraft and lead to more sophisticated results especially for flight cases close to stall. In addition to the model for the longitudinal motion the lateral motion model will be added and simulations will be performed. It is planned to perform research on asymmetric flight cases with active high lift systems, engine failures and control efficiency of the lateral control devices. Later on safety issues and resulting safety margins will be analyzed.

ACKNOWLEDGEMENTS

This project is part of the “Sonderforschungsbereich 880”, therefore the author would like to thank the German Research Foundation (DFG) for supporting this research as fundamental research for active high lift augmented flight systems. The author would like to thank Dipl.-Ing. Dennis Keller from DLR (Institute of Aerodynamics and Flow Technology), Dipl.-Ing. Tayson Weiss from TU Braunschweig (Institute of Aircraft Design and Lightweight structures), and M. Sc. Marco Burnazzi from TU Braunschweig (Institute of Fluid Mechanics) for providing the aerodynamic data. Dr.-Ing. Wolfgang Heinze from TU Braunschweig (Institute of Aircraft Design and Lightweight structures) should also be thanked for providing the RAC and main aircraft data.

LITERATURE

[1] W. J. Crowther, M. Jabbal, S. C. Liddle: “Flow control fallacies: a review of common pitfalls in flow control research”, Proceedings of the Institution of Mechanical Engineers, Part G: Journal of Aerospace Engineering, vol. 225, no. 1, pp. 1–11, 2011.

[2] B. Norton: “STOL progenitors: The technology path to a large STOL transport and the C-17A”, Book, ISBN 1-56347-576-6, Publ.: American Institute of Aeronautics and Astronautics, Inc., Reston, Va, 2002.

[3] C. Werner-Westphal, W. Heinze, P. Horst: “Multidisciplinary Integrated Preliminary Design Applied to Future Green Aircraft Configurations”, AIAA 2007-655, 45th AIAA Aerospace Sciences Meeting and Exhibit, vol. 2007, Jan. 2007.

[4] https://www.tu-braunschweig.de/ifl/forschung /flugzeugvorentwurf, Preliminary Aircraft Design completed projects, Latest version: 10:30 am, Jul 6, 2012.

[5] C. Raab: A Versatile and Modular Architecture for Aircraft System Simulation and Test, Institute Report IB 111-2006/22, Institute of Flight Systems, DLR, Braunschweig, Jul, 2006.

[6] K.-C. Pfingsten, R. Radespiel: “Use of upper surface blowing and circulation control for gapless high lift configurations”. In: CEAS/KATnet Conference on Key Aerodynamic Technologies, Bremen, Jun 20–22, 2005.

[7] R. J. Englar: “Development of Pneumatic Aerodynamic Devices to Improve the Performance, Economics, and Safety of Heavy Vehicles”. In SAE TECHNICAL PAPER SERIES, Washington, D.C., Jun 19-21, 2000.

[8] R. Brockhaus, W. Alles, R. Luckner: „Flugregelung“, 3rd ed., ISBN 978-3-642-01442-0 Publ.: Springer, Berlin, 2010.

[9] R. V. Jategaonkar: “Flight Vehicle System Identification: A Time Domain Methodology, Progress in Astronautics and Aeronautics”, ISBN 1-56347-836-6, Publ.: American Institute of Aeronautics and Astronautics, Reston, Va, 2006.

[10] W. Mönnich: „Ein 2-Punkt-Aerodynamikmodell für die Identifizierung“, In: „Systemidentifikation in der Fahrzeugdynamik“: Symposium des Sonderforschungs-bereichs SFB 212 "Sicherheit im Luftverkehr", Braunschweig, Mar 10-11, 1987.

[11] H. Schlichting, E. Truckenbrodt: „Aerodynamik des Flugzeuges, Zweiter Band“, 2nd ed., ISBN 3-540-04700-X, Publ.: Springer, Berlin, 1969.

APPENDIX

Parameter	Unit	Case 1	Case 2	Case 3	Case 4	Case 5
Weight	kg	36061	40641 (MTOW)	40641 (MTOW)	38901 (MLW)	36061
V_{TAS}	m/s	220.0	109.7	81.38	44.140	43.0
M	-	0.74	0.33	0.24	0.13	0.13
Alt	m	10600.0	1524	1524	100	100
FPA	deg	0.0	0.0	0.0	0.0	0.0
α	deg	0.86	4.0	10.0	4.0	2.85
α_{HTP}	deg	-0.6	-0.3	0.8	-12.1851	-12.72
i_{HTP}	deg	1.93	0.11	-2.6957	0.32	0.70
$Throttle$	%	29.68	11.1558	12.85	34.38	31.76
$Flaps$	deg	0.000	0.0	0.0	65.0	65.0
C_{μ}	-	-	-	-	0.040	0.0425

TAB. 2 Trim points for different flight cases